Available online at www.sciencedirect.com
ScienceDirect
Acta Biomaterialia 3 (2007) 113–119
Acta BIOMATERIALIA
www.actamat-journals.com

Surface elastic properties of Ti alloys modified for medical implants: A force spectroscopy study

Carmen Munuera [a], Thomas Reinhold Matzelle [b], Norbert Kruse [b], María Francisca López [a], Alejandro Gutiérrez [c], José Antonio Jiménez [d], Carmen Ocal [a,b,*]

[a] Instituto de Ciencia de Materiales de Madrid, CSIC, Cantoblanco, E-28049 Madrid, Spain
[b] Chemical Physics of Materials, Université Libre de Bruxelles, La Plaine CP243, B-1050 Brussels, Belgium
[c] Departamento de Física Aplicada, Universidad Autónoma de Madrid, Cantoblanco, E-28049 Madrid, Spain
[d] Centro Nacional de Investigaciones Metalúrgicas, CSIC, Avda. Gregorio del Amo 8, E-28040 Madrid, Spain

Received 19 May 2006; received in revised form 31 July 2006; accepted 23 August 2006

Abstract

We report here the first nanoscale surface elasticity measurements on surface-modified titanium alloys using the force spectroscopy mode in scanning force microscopy. Samples of three vanadium-free titanium alloys, Ti–7Nb–6Al, Ti–13Nb–13Zr and Ti–15Zr–4Nb, were investigated. Surface modification of the three alloys was produced by thermal oxidation in air at 750 °C for different times, which resulted in the formation of protective oxide layers with different surface composition and morphology. The elastic properties of the surface layers were studied comparatively in the as-received Ti alloys and after the oxidation process using cantilevers with different stiffness to evaluate the influence of the indentation depth. In all cases, Young's modulus of the sample surfaces was found to be lower than 65 GPa, and as low as 20 GPa for some of the oxidized samples. Variations observed for the three oxidized Ti alloys can be related to the different chemical composition of the outer layers generated for the different oxidation times.

Keywords: Nanoindentation; SFM (scanning force microscopy); Biomaterials; Metal alloy; Elastic behavior

1. Introduction

Their high strength-to-weight ratio and low elastic modulus combined with a satisfactory corrosion behavior make titanium and titanium-based alloys outstanding biomaterials and promising candidates for the replacement of hard tissues such as those present in artificial hip joints or dental implants. The spontaneous development of a stable and protective passive layer with a thickness of a few nanometers when exposed to an oxygen-containing atmosphere provides these materials with a high biocompatibility associated with a high corrosion resistance in aggressive biological environments. During the past 50 years the standard alloy for these purposes has been Ti–6Al–4V, but it has been recently reported that the release of vanadium ions from the alloy might cause health problems due to their toxicity [1]. For this reason, there is growing research activity aimed at developing vanadium-free titanium alloys for biomedical applications presenting a good combination of biocompatibility, corrosion resistance and mechanical properties similar to those of Ti–6Al–4V. Within this approach, three α–β Ti alloys of composition (in wt.%) Ti–7Nb–6Al, Ti–13Nb–13Zr and Ti–15Zr–4Nb, proposed as potential biomaterials, have been previously characterized [2,3]. In those works, the in vitro corrosion behavior of the alloys, immersed in Hanks' solution, as well as the microstructure and chemical composition of the passive layer spontaneously formed in air, were studied. The electrochemical investigations pointed to a similar corrosion

* Corresponding author. Address: Instituto de Ciencia de Materiales de Madrid, CSIC, Cantoblanco, E-28049 Madrid, Spain. Tel.: +34 91 334 90 23.
E-mail address: carmenocal@icmm.csic.es (C. Ocal).

1742-7061/$ - see front matter © 2006 Acta Materialia Inc. Published by Elsevier Ltd. All rights reserved.
doi:10.1016/j.actbio.2006.08.009

resistance for the three alloys, with values lower than those obtained for Ti–6Al–4V. The microstructural study revealed the existence of two different phases, α and β, with the α/β ratio being dependent on the alloy composition. Thus, the Ti–13Nb–13Zr alloy surface is rich in the β-phase due to a high content of Nb, a β-stabilizer element. Meanwhile, as Al is an α-stabilizer, and Zr is neutral, both Ti–7Nb–6Al and Ti–15Zr–4Nb surfaces are richer in α-phase.

One way to improve corrosion prevention and wear resistance in titanium alloys would be to increase the thickness of the passive layer. In order to do that, we have used a simple thermal treatment in air at 750 °C to generate a highly protective, bioinert oxide layer on the alloys' surface. Previously to the present study, complementary techniques had already been used to investigate some properties of these layers. In particular, characterization by soft X-ray absorption spectroscopy (XAS), X-ray photoelectron spectroscopy (XPS), Rutherford backscattering spectroscopy (RBS) and elastic recoil detection (ERD) showed differences in composition of the oxide layer grown on the three alloys [4,5]. The passive Ti_2O_3 oxide layer formed on the as-received Ti–7Nb–6Al surface evolves, after an oxidation time of 1.5 h, into an Al_2TiO_5 layer on top of which an Al_2O_3 layer grows and thickens with further oxidation time. However, for the two TiNbZr alloys a TiO_2 rutile layer is formed on the alloy surface independently of the oxidation time. Cross-sectional scanning electron microscopy (SEM) and electrochemical measurements were also performed to follow the development of the layer as a function of the oxidation time and to investigate the protective character of the oxidized layers against corrosion [6]. More recently, we have conducted a scanning force microscopy (SFM) study that reveals a correlation between roughness, oxidation time and surface composition of these oxide layers [7]. In the present study we attempt a further characterization of these layers by determining their nanoscale elastic properties.

Despite the great progress that has been achieved in producing orthopedic biomaterials, one of the major reasons for implant loosening following stress shielding in bones is the mismatch between the Young's moduli of the biomaterials employed (between 110 GPa for Ti and 230 GPa for Co–Cr alloys) and the surrounding bone (10–30 GPa). Therefore, the elastic characterization of the outermost layers, which may present different elastic properties than the bulk and are those in direct contact with the bone, is crucial when suggesting alternative alloys.

We report here the results obtained using SFM in the force spectroscopy mode to investigate the elastic modulus in the very outermost layers of the aforementioned surface-modified Ti alloys. In recent years SFM has become a powerful technique for the study of the nanoscale surface structure of materials. In addition to the topographic analysis, the sensitivity of SFM to sub-nano-Newton forces has led to its use in the characterization of surface properties such as friction, adhesion and elastic modulus. In the latter case, force vs. distance curves measured with the SFM tips lead to indentation curves and, by analogy with classical indentation techniques, the respective surface moduli can be obtained [8–12].

Validation of the elastic moduli obtained in the present work is discussed by comparing data obtained with cantilevers of different stiffness and by assessing the non-invasive character of the technique in the force regime employed, where neither wear nor plastic deformation occurred as confirmed by SFM imaging verification. Furthermore, by taking advantage of the imaging capability of the SFM, we have analyzed the correlation between nanoscale elasticity and surface characteristics.

2. Experimental

2.1. Materials and sample preparation

The Ti-based alloys of composition (in wt.%) Ti–7Nb–6Al (T1), Ti–13Nb–13Zr (T2) and Ti–15Zr–4Nb (T3) were prepared as explained elsewhere [2]. The sample surface was abraded and polished using diamond pastes with successively finer particle size. In the final stage, colloidal silica was used to ensure a surface free of mechanical deformation. The material in this state is the as-received sample. For each composition, four different samples were investigated: the as-received one, exhibiting a thin native oxide layer, and three samples after oxidation treatments at 750 °C in air for 1.5, 6 and 24 h. At the final stage, the oxide layers were 2, 10 and 25 μm in thickness for T1, T2 and T3, respectively, as determined by SEM cross-sectional observations [6].

2.2. Scanning force microscopy and force spectroscopy

SFM measurements were performed using a commercial scanning force microscope (TMX 2100 Explorer, TopomeMetrix, now Veeco Metrology, Santa Barbara, CA).[1] Two types of Ultralever, V-shaped, Si_3N_4 probes (Park Scientific Instruments, now also Veeco Metrology) with nominal spring constants (k) of 0.4 and 2.1 N/m, respectively, were used. Since actual spring constants can differ from their nominal values, the cantilevers were calibrated using the "reference-spring method" [13], which revealed an accuracy of 0.08 N/m. Furthermore, particular attention was given to the estimation of the tip radius, which is an essential parameter in our elasticity analysis. The probe was characterized by field emission scanning electron microscopy (FESEM) and a half opening angle of approximately 12.5° and a radius of about 15 nm were obtained [14]. This holds for all Ultralever tips used in the experiments.

In order to ensure grease-free and dust-free surfaces, the samples were cleaned in an acetone ultrasonic bath for 10

[1] For details of the experimental set-up (photographs and schematics), see http://electron.mit.edu/~gsteele/mirrors/elchem.kaist.ac.kr/jhkwak/TopometrixWeb/TopoHome.htm.

min prior to each measurement and placed in a home-made cell to perform SFM. All experiments were carried out in deionized water, reducing any possible electrostatic interaction and avoiding the adhesion force which appears, due to the formation of a water meniscus, between tip and sample when measuring in air. Measuring under liquid conditions then allows a more accurate analysis of the applied forces and, consequently, of the calculated mechanical properties of the Ti alloys. In addition, measurements in water are closer to physiological conditions than those performed in air.

In all cases, the experimental procedure was as follows: a topographic image of the respective Ti alloy surface (up to 50 μm lateral size) was taken in the contact mode and, subsequently, force–distance curves were recorded on selected locations of the surface. To assess any deterioration in the tip response, force–distance curves were also measured on a mica surface (prior and after measuring on the sample), which served as a reference. Once the reference curve was established, the same tip and the same position of the laser spot on the cantilever were kept unchanged throughout the measurements of the whole sample series. The applied force was maintained in the nano-Newton range to minimize any tip or sample damage and to ensure indentation experiments were carried out in the elastic regime. Tip conditions and the absence of any detectable plastic deformation were verified by topographic imaging (prior and after elasticity measurements) and lack of hysteresis in the trace/retrace force vs. distance curves.

Under these conditions, i.e., before plastic deformation occurs, the indentation of the SFM tip into a relatively soft sample can be modeled by using Hertzian contact mechanics to provide a simple yet direct approach to the sample elasticity properties. Following the procedure described first by Radmacher and co-workers [8], the indentation curve of a material surface can be obtained by comparing the slope of the force vs. distance curve of this material with that of a hard surface. As the surface of the hard material is not indented by the tip, the cantilever deflection is proportional to the z-piezo movement and, therefore, the force vs. displacement curve has a constant slope as soon as the tip contacts the surface. However, on a compliant material the tip indents into the sample and the same cantilever deflection is obtained only after an additional piezo travel. This is shown in Fig. 1(a), where deflection vs. distance curves are plotted for mica and the T1 alloy. The indentation (δ) at a given deflection value is given by the extra z-piezo motion needed to achieve the same cantilever deflection as on the hard material. The calculated indentation values are plotted in Fig. 1(b) as a function of the applied force, which is directly obtained multiplying the cantilever deflection by the spring constant.

For small indentation depths, the Hertzian model of a sphere–plane contact is routinely applied to fit the experimental indentation vs. load curves. According to the Hertz theory:

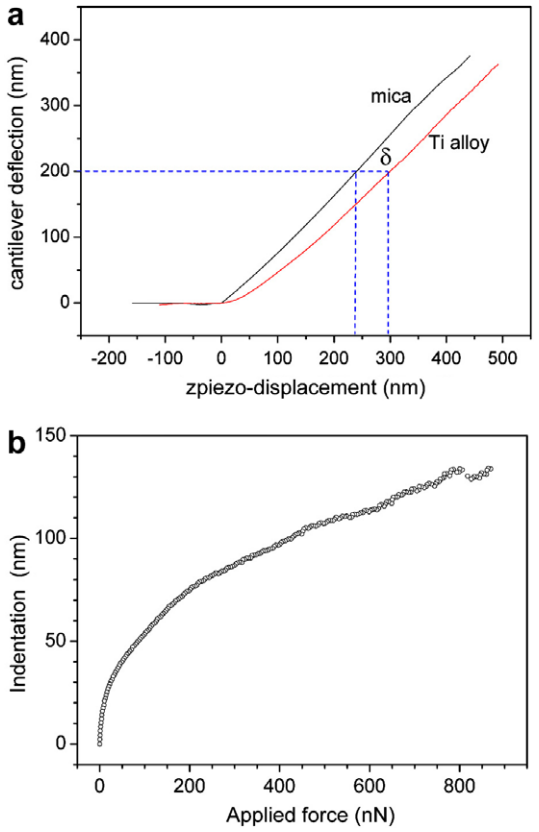

Fig. 1. (a) Force vs. displacement curves on a freshly cleaved mica surface and on the as-received Ti–7Nb–6Al sample surface (traces only). An equal displacement of the z-piezo results in a smaller cantilever deflection on the titanium alloy surface compared to the mica surface due to elastic indentation. (b) Indentation vs. applied force curve calculated from the curves in (a).

$$\delta = \left(\frac{3}{4}\frac{f_{\text{sphere}}}{E^*\sqrt{R}}\right)^{\frac{2}{3}}, \tag{1}$$

where δ is the indentation, f_{sphere} the load applied by the tip, R the tip radius and E^* the reduced Young modulus, given by

$$\frac{1}{E^*} = \frac{(1-\nu_{\text{tip}}^2)}{E_{\text{tip}}} + \frac{(1-\nu_{\text{sample}}^2)}{E_{\text{sample}}} \tag{2}$$

In this equation, ν_{sample} and ν_{tip} stand for the Poisson ratios, and E_{sample} and E_{tip} for the Young's modulus of sample and tip, respectively.[2] Therefore, Young's modulus of the samples can be extracted from the fits to the experimental data. Note that the model is valid only if $E_{\text{tip}} > E_{\text{sample}}$ and, as will be discussed below, care has to be taken in applications where $E_{\text{tip}} \approx E_{\text{sample}}$.

[2] The values of the Poisson ratio used to calculate E have been chosen according to the studies of the chemical composition of the sample surface. They ranged from 0.235 to 0.3. For Si_3N_4 cantilevers the elasticity value is $E_{si} = 150$ GPa and the Poisson ratio is $\nu = 0.27$.

3. Results and discussion

A thorough investigation of the oxide layer topography as a function of the oxidation time of the three alloy materials including careful root mean square (rms) analysis has been previously reported [7]. The effect of the oxidation treatment on the surface morphology is seen in SFM images, such as those in Fig. 2(a)–(c). Since the morphological structure of some surfaces presents significant inhomogeneities on large-scale areas (>25 μm^2), in order to have suitable locations for measuring force vs. distance curves, low-roughness regions (<0.5 μm^2) were chosen by SFM imaging prior to elasticity measurements.

In Fig. 2(d) typical deflection vs. z-piezo displacement curves (traces only) are shown for the complete T1 series. A comparison of the curves for bare mica (black) with those for the Ti alloys (gray) demonstrates that the alloys are soft enough to be elastically deformed under the low forces applied so as to determine their elastic modulus according to the procedure described in Section 2. A similar set of curves was obtained for the T2 and T3 series as well. A total of about 200 curves, i.e. more than 15 for each sample, were measured.

There is common agreement that indentation measurements on thin films are influenced by the elastic properties of the underlying material unless the ratio of the indentation depth to film thickness is small enough to neglect the effect of the substrate [15]. As endorsed by previous studies, in the present case this condition is fulfilled for all the samples, since indentation values are kept much smaller than the thickness of the oxide layers under investigation [6]. However, possible differences in the elastic behavior may exist due to changes in the stoichiometry, composition and structure of the oxide layers when going deep into the surface, and these differences can be addressed by sampling different force regimes.

The applied forces were below ~100 nN for cantilevers with $k = 0.4$ N/m, whereas for stiffer cantilevers ($k = 2.1$ N/m) the applied forces reached values up to 10 times higher, thus allowing deep penetration into the mate-

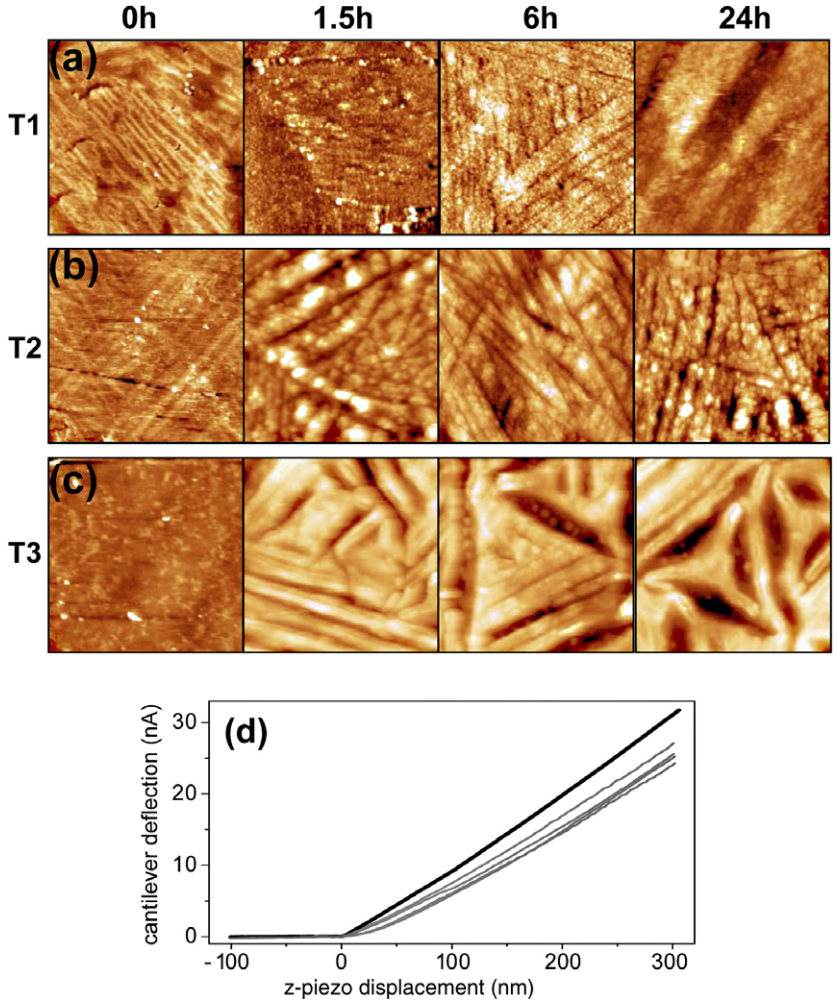

Fig. 2. SFM topographic images (20 μm lateral size) of (a) Ti–7Nb–6Al, (b) Ti–13Nb–13Zr and (c) Ti–15Zr–4Nb in their as-received state (0 h) and after the oxidation treatment at 750 °C for 1.5, 6 and 24 h. (d) Typical deflection vs. z-piezo displacement curves measured on the mica surface (black) and on the Ti–7Nb–6Al (T1) series (gray).

rial. This is shown in Fig. 3, where two indentation curves are depicted for T2 after an oxidation treatment of 1.5 h. The applied forces are one order of magnitude higher for the stiffer cantilever (b). Although, consequently, the indentation values increase, neither significant indentation nor plastic deformation occurs and the Hertzian contact theory can be applied. The indentation curves corresponding to measurements performed with the soft cantilever (Fig. 3(a)) can be described with high accuracy by using the Hertzian model for a sphere–plane contact for the whole indentation range (continuous line). On the other hand, the curve measured for the stiff cantilever shown in Fig. 3(b) presents two different regimes which can be separately fitted by the Hertz model. The elastic modulus derived from the fit for small indentation values and small applied forces (steep line) agrees, within the error, with that obtained for the low-stiffness cantilever for the same load range. However, values of E obtained from data at high loads (see fit in this regime) have no physical meaning. We note that the same method was successfully employed to probe soft materials, such as polymers, fibers and organic lubricants, where the limitation $E_{\text{tip}} \approx E_{\text{sample}}$ is never reached. However, the difference in Young's modulus between tip and the surfaces investigated here is not so large and, as mentioned in Section 2, the method fails for high loads.

Taking into account these considerations, we have compared the values of Young's modulus obtained from the entire curve fit, in the case of the softer cantilever, and from the fit to the same force range in the curve obtained with the stiffer cantilever. These values are plotted in Fig. 4 and, within the error bars, are found to be quite similar along the T1 and T2 series. The largest dispersion observed for the third series can be accounted for by the morphological structure of the T3 samples. As can be seen in Fig. 2(c), the oxide layer formed in the T3 alloy after all the thermal treatments exhibits a characteristic triangular microstructure with considerable differences in topographic levels, such as grooves (up to 500 nm deep) and ridges, which provide an overall surface roughness of about 250 nm in terms of the rms regardless of the oxidation time [7]. Although care was taken to keep the influence of these morphological features on the indentation low, measurements free of any such convolution are hardly possible. Wherever the sample was probed, a large rms of the topmost surface was obtained, reflecting a particular microstructure and influencing the respective force vs. distance curves with different cantilevers. Clearly, while increasing the load, both the uncertainty on the true indentation depth and the true contact area likewise increase.

Although no direct correlation between the Young's modulus and the oxidation time for the different alloys can apparently be inferred from Fig. 4, some relationships can be derived when considering the evolution of the oxide composition and the α/β phase ratios [4].

We note first the differences in the initial value of E for each alloy, which corresponds to the as-received surfaces covered by a passive layer of Ti_2O_3 composition [4]. A lower α/β ratio seems to be the origin of the high E value measured for T2-0, whereas T1-0 and T3-0 present similar E values, corresponding to their similar α/β ratios [3].

By considering the variations observed as a function of oxidation time, we note that the sudden increase in E observed for the Al-containing alloy after 1.5 h of thermal treatment (T1-1.5 in Fig. 4) seems to be related to the evolution of the Ti_2O_3 oxide layer formed on the as-received sample to a layer of Al_2TiO_5 composition. The growth of a defective Al_2O_3 layer on top of it, observed for T1 at 6 h, implies a decrease of E, while the final increase in thickness of this layer, which almost certainly becomes less porous, gives rise once more to higher E values for T1-24.

The decrease of E from T2-0 to T2-1.5 would then be related to the conversion from Ti_2O_3 to TiO_2 as concluded in Ref. [4]. As in the former case, the observed increase in E might be justified if, as expected, thickening of the outer oxide layer is accompanied by a loss of porosity. The formation of thick and compact oxide layers from the initial oxidation of T3 seems to be the reason for the rather similar and low E values measured for the whole oxidation time period studied here.

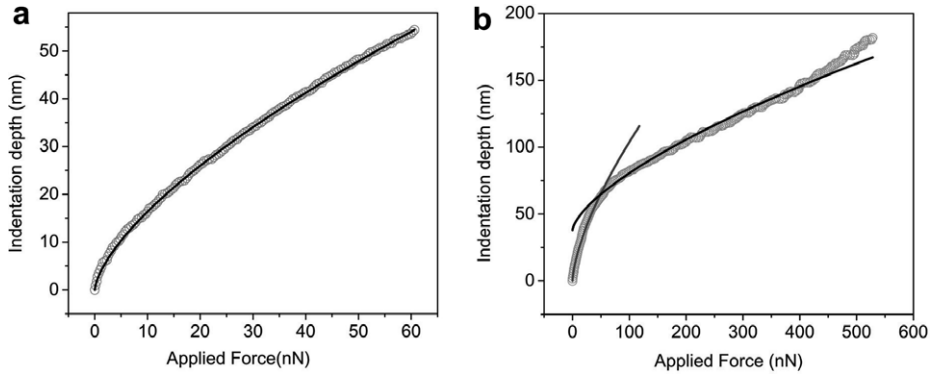

Fig. 3. Indentation as a function of the loading force for Ti–13Nb–13Zr (T2) after the oxidation treatment for 1.5 h, for cantilevers of two spring constants: $k = 0.4$ N/m (a) and $k = 2.1$ N/m (b). Solid lines correspond to the Hertz theory fits for a small sphere indenting a plane surface. Low- and high-indentation regimes are fitted in (b); see the text for interpretation.

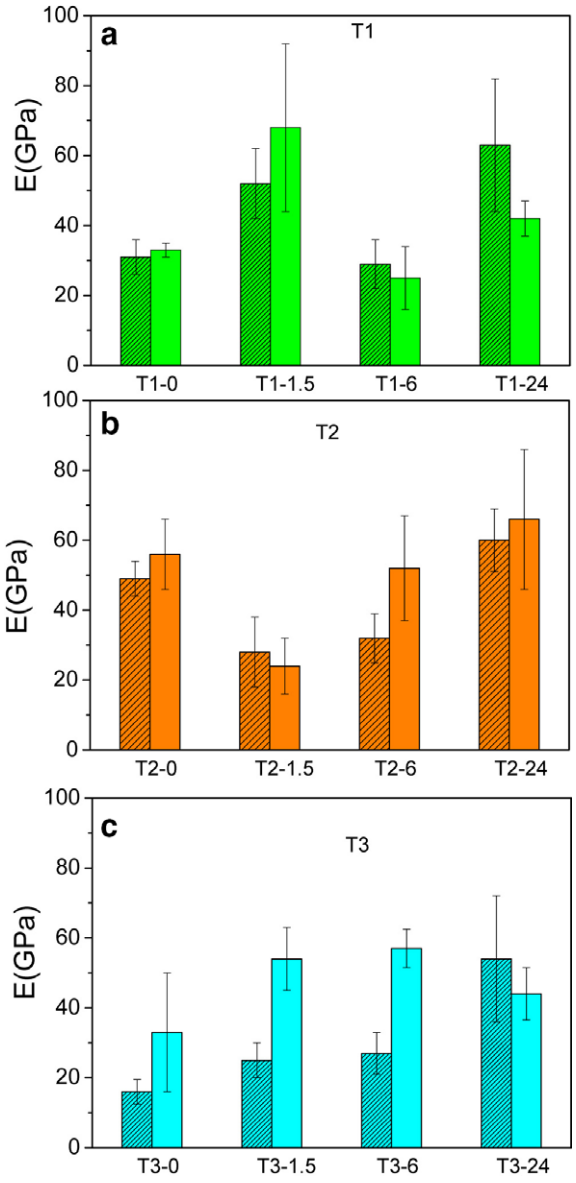

Fig. 4. Experimental values of Young's modulus (in GPa) for (a) T1, (b) T2 and (c) T3 series. Shaded bars represent the values obtained from the fits to the entire curve obtained with the $k = 0.4$ N/m cantilever. Plain colored bars represent the values obtained from the fit to the same load regions (low forces) of the indentation curves measured with the $k = 2.1$ N/m cantilever.

On average, the resulting Young's moduli are lower than 65 GPa and, in some cases, the elastic modulus is as low as 20 GPa. In all cases, the values are remarkably lower than the Young's modulus of Ti–6Al–4V (108 GPa) [16], which is the most widely used titanium alloy. The values are also significantly lower than those found in the literature [1,17–19] for similar Ti alloys after different surface treatments. This does not come as a surprise since different results must be expected from different penetration depth techniques [20]. In our measurements, the outermost layers of the sample surface are probed, and in most reported cases, much larger indentations have been recorded.

4. Conclusions

The elastic properties of three different Ti alloys in their as-received state and after oxidation treatments in air at 750 °C have been studied to investigate their suitability as implant materials. By means of SFM we have obtained indentation curves and, by applying the Hertz model, we have calculated the Young's modulus for all the samples. The values obtained with this technique are representative of the outermost layers of the alloy surfaces, which are crucial for the success of implant biocompatibility.

Cantilevers with different stiffnesses were used to investigate differences in the elastic properties as a function of the indentation depth. Although we have observed a different response of the Young's modulus as the tip penetrates into the material, a quantitative analysis for this deep-layer penetration is not possible since E_{sample} becomes similar to E_{tip} so that the applied model is no longer valid.

For sampling depths of less than 60 nm, the SFM measurements reveal that, in all cases, the values of the Young's modulus lie below 65 GPa, and are as low as 20 GPa for some oxidized samples. This value is very close to that of bone. Based on previous studies, the α/β ratios of the as-received samples as well as the evolution of the composition of the outermost oxide layers developed on the different alloy surfaces are proposed as a plausible explanation for the variation of Young's moduli for the three samples.

The results presented in this work show that an extremely surface-sensitive technique such as SFM in its force spectroscopic mode can be used to investigate the elastic behavior of highly protective, bioinert oxide layers developed on Ti alloys. These oxide layers offer suitable alternatives for medical implants, and can be made economically by oxidation in air.

Acknowledgements

We are greatly indebted to Professor G. Frommeyer from the Max Planck Institut für Eisenforschung (Düsseldorf) for kindly supplying the Ti alloy specimens. This work has been supported by Project MAT-2004-00150 of the Spanish MEC and Projects 07N-0050-1999 and 07N-0066-2002 of the Spanish "Programa de Tecnología de los Materiales de la Comunidad Autónoma de Madrid" and the European Union FEDER program. A.G. and C.O. thank the Spanish MEC for financial support through the "Ramón y Cajal" and the "Formation and Mobility" (Ref. PR2004-0425) Programs. C.M. thanks the CSIC for a I3P scholarship.

References

[1] Okazaki Y, Rao S, Ito Y, Tateishi T. Corrosion resistance, mechanical properties, corrosion fatigue strength and cytocompatibility of new Ti alloys without Al and V. Biomaterials 1998;19(13):1197.

[2] López MF, Jiménez JA, Gutiérrez A. Surface characterization of new non-toxic titanium alloys for use as biomaterials. Surf Sci 2001;482–485:300.
[3] López MF, Jiménez JA, Gutiérrez A. In vitro corrosion behaviour of titanium alloys without vanadium. Electrochim Acta 2002;47:1359.
[4] López MF, Soriano L, Palomares FJ, Sánchez-Agudo M, Fuentes GG, Gutiérrez A, et al. Soft X-ray absorption spectroscopy study of oxide layers on titanium alloys. Surf Interf Anal 2002;33:570.
[5] Gutiérrez A, López MF, Jiménez JA, Morant C, Paszti F, Climent A. Surface characterization of the oxide layer grown on Ti–Nb–Zr and Ti–Nb–Al alloys. Surf Interf Anal 2004;36:977.
[6] López MF, Jiménez JA, Gutiérrez A. Corrosion study of surface-modified vanadium-free titanium alloys. Electrochim Acta 2003;48:1395.
[7] Gutiérrez A, Munuera C, López MF, Jiménez JA, Morant C, Matzelle T, et al. Surface microstructure of the oxide protective layers grown on vanadium-free Ti alloys for use in biomedical applications. Surf Sci; in press.
[8] Radmacher M, Fritz M, Hansma PK. Imaging soft samples with the atomic force microscope: gelatin in water and propanol. Biophys J 1995;69:264.
[9] Stark RW, Drobek T, Weth M, Fricke J, Heckl WM. Determination of elastic properties of single aerogel powder particles with the AFM. Ultramicroscopy 1998;75:161.
[10] Reynaud C, Sommer F, Quet C, El Bounia N, Duc TM. Quantitative determination of Young's modulus on a biphase polymer system using atomic force microscopy. Surf Interf Anal 2000;30:185.
[11] Matzelle TR, Ivanov DA, Landwer D, Heinrich LA, Herat-Bruns Ch, Reichelt R, et al. Micromechanical properties of "smart" gels: studies by scanning force and scanning electron microscopy of PNIPAAm. J Phys Chem B 2002;106:2861.
[12] Shulha H, Kovalev A, Myshkin N, Tsukruk VV. Some aspects of AFM nanomechanical probing of surface polymer films. Eur Poly J 2004;40:949.
[13] Torii A, Sasaki M, Hane K, Okuma S. A method for determining the spring constant of cantilevers for atomic force microscopy. Meas Sci Technol 1996;7:179.
[14] Matzelle TR, Kruse N, Reichelt R. Characterization of the cutting edge of glass knives for ultramicrotomy by scanning force microscopy using cantilevers with a defined tip geometry. J Microscopy 2000;199:239.
[15] Huang H, Winchester K, Liu Y, Hu XZ, Musca CA, Dell JM, et al. Determination of mechanical properties of PECVD silicon nitride thin films for tunable MEMS Fabry-Pérot optical filters. J Micromech Microeng 2005;15:608.
[16] Pilliar RM. Modern metal processing for improved load-bearing surgical implants. Biomaterials 1991;12:95.
[17] Kuroda D, Niinomi M, Morinaga M, Kato Y, Yashiro T. Design and mechanical properties of new β type titanium alloys for implant materials. Mater Sci Eng A 1998;243:244.
[18] Tang F, Awane T, Hagiwara M. Effect of compositional modification on Young's modulus of Ti_2AlNb-based alloy. Scripta Mater 2002;46:43.
[19] Niinomi M. Fatigue performance and cyto-toxicity of low rigidity titanium alloy, Ti–29Nb–13Ta–4.6Zr. Biomaterials 2003;24:2673.
[20] Radovic M, Lara-Curzio E, Riester L. Comparison of different experimental techniques for determination of elastic properties of solids. Mater Sci Eng A 2004;368:56.